

Effect of laser frequency fluctuation on the decoherence rate of Rydberg polaritons

Bongjune Kim,¹ Ko-Tang Chen,¹ Chia-Yu Hsu,¹ Shih-Si Hsiao,¹ Yu-Chih Tseng,¹ Chin-Yuan Lee,¹ Shih-Lun Liang,¹ Yi-Hua Lai,¹ Julius Ruseckas,² Gediminas Juzeliūnas,² and Ite A. Yu^{1,3,*}

¹*Department of Physics, National Tsing Hua University, Hsinchu 30013, Taiwan*

²*Institute of Theoretical Physics and Astronomy,*

Vilnius University, Saulėtekio 3, LT-10222 Vilnius, Lithuania

³*Center for Quantum Technology, Hsinchu 30013, Taiwan*

(Dated: December 15, 2024)

The effect of electromagnetically induced transparency (EIT) using Rydberg-state atoms provides high optical nonlinearity to effectively mediate the photon-photon interaction. However, the decoherence rate of Rydberg polaritons, which plays an important role in the efficiency of optical nonlinear, can be largely influenced by the laser frequency fluctuation. In this work, we carry out a systematic theoretical and experimental study of effects of the laser frequency fluctuation on the EIT. We analyze a theoretical model that quantitatively describes the relationship between the decoherence rate and laser frequency fluctuation. The derived theoretical formula was experimentally verified for the Λ -type EIT system of laser-cooled ^{87}Rb atoms, in which one can completely eliminate or controllably introduce the laser frequency fluctuation. We further extended the formula to include the effect of the Doppler shift due to the atomic motion, and measured the decoherence rate in the Rydberg-EIT system. The measurement was carried out using ^{87}Rb atoms cooled to 350 μK and with the Rydberg state of $|32D_{5/2}\rangle$ involved. We achieved a rather low decoherence rate of $2\pi \times 48$ kHz at a moderate coupling Rabi frequency of $2\pi \times 4.3$ MHz. The experimental data are consistent with the theoretical predictions.

I. INTRODUCTION

Currently there is a great deal of interest in utilizing of strong dipole-dipole interactions (DDI) between Rydberg-state atoms in the applications of quantum information manipulation with photons, such as realization of quantum logic gates [1–3], generation of single photons [4, 5], quantum simulations [6, 7], etc. These applications are made feasible by the DDI-induced blockade effect, the phenomenon that multiple excitation to a Rydberg state within blockade radius is strongly suppressed [8–17]. The effect of electromagnetically induced transparency (EIT) provides high nonlinearity for photons [18–20]. Hence, the combination of the EIT effect and Rydberg-state atoms can effectively mediate the photon-photon interaction at single-photon level, offering a powerful tool for quantum information processing of photonic qubits [21–28]. Storage of light based on the EIT effect prolongs the atom-photon or photon-photon interaction time and further enhances the optical nonlinear efficiency [29–36]. Owing to long life times of Rydberg states, the nonlinear efficiency enhanced by the EIT storage is also practical in the Rydberg-EIT system. All-optical switching and cross-phase shift of π with single photons [31, 32] and single-photon subtraction [36] have been demonstrated with the Rydberg-EIT storage.

A Rydberg polariton is a collective excitation involving the light and the atomic coherence between the ground state and the Rydberg state. In a typical EIT or slow light experiment, the Rydberg polaritons represent

mostly the atomic Rydberg excitations (Rydberg coherences), and there is only a tiny photonic contribution to the polariton, like the polaritons involving the usual Λ -type EIT [37, 38]. Therefore, we will not distinguish the polariton from the atomic coherence in this paper. In particular, the decoherence rate of the Rydberg polariton just means the dephasing rate of the coherence between the atomic Rydberg and ground states. Since the decoherence rate can greatly influence optical nonlinear efficiency in the Rydberg-EIT system [39–43], laser frequency fluctuation increases the Rydberg-polariton decoherence rate and deteriorates the efficiency. Hence, the laser frequency fluctuation can be a problem in the study of high-fidelity low-loss quantum processes utilizing the Rydberg polariton.

The Λ -type EIT (abbreviated as Λ -EIT) system consists of two ground states and one excited state driven by the probe and coupling fields as shown in Fig. 1(a), where the two ground states have a frequency difference typically less than 10 GHz. Using the phase-lock or injection-lock scheme, one can maintain the frequency difference between the two laser fields constant. Consequently, the two-photon laser frequency of the Raman transition (i.e., the difference of two laser frequencies) is stabilized to a high degree, and the problem of laser frequency fluctuation can be completely eliminated in the Λ -EIT system. On the other hand, the Rydberg-EIT system consists of one ground state, one intermediate excited state, and one Rydberg state driven by the probe and coupling fields as shown in Fig. 1(b). The two laser fields typically have very different colors. For example, in the case of Rb atoms, the probe field has a wavelength of about 780 or 795 nm and the coupling field has a wavelength in the range between 474 and 484 nm. The schemes of

*Electronic address: yu@phys.nthu.edu.tw

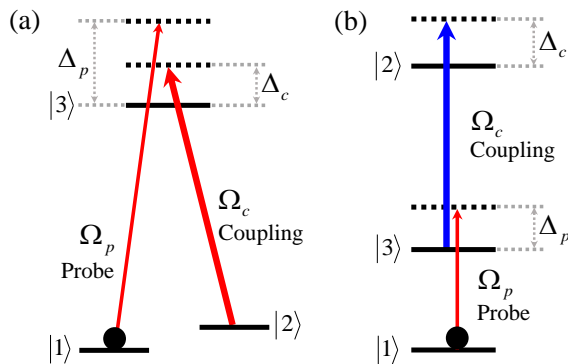


FIG. 1: Relevant energy levels and laser excitations in the Λ -EIT system are shown in (a) and those in the Rydberg-EIT system are shown in (b). We employed laser-cooled ^{87}Rb atoms in the experiment. In (a), states $|1\rangle$ and $|2\rangle$ correspond to the ground states $|5S_{1/2}, F=1, m_F=1\rangle$ and $|5S_{1/2}, F=2, m_F=1\rangle$, and state $|3\rangle$ corresponds to the excited state $|5P_{3/2}, F=2, m_F=2\rangle$. In (b), states $|1\rangle$, $|2\rangle$, and $|3\rangle$ correspond to the ground state $|5S_{1/2}, F=2, m_F=2\rangle$, the Rydberg state $|32D_{5/2}, m_J=5/2\rangle$, and the excited state $|5P_{3/2}, F=3, m_F=3\rangle$, respectively. A weak probe field of the Rabi frequency Ω_p drives a transition of $|1\rangle \rightarrow |3\rangle$ with a detuning Δ_p . A strong coupling field of Ω_c couples states $|2\rangle$ with $|3\rangle$ with a detuning Δ_c . Hence, the two-photon detuning δ is $\Delta_p - \Delta_c$ in (a) and is $\Delta_p + \Delta_c$ in (b).

reference cavities, high-resolution wavemeters, and EIT signals with hot vapor cells have been employed for the stabilization of laser frequencies in the Rydberg-EIT system [44–46]. However, the two-photon laser frequency of the Rydberg transition (i.e., the sum of the probe and coupling frequencies) stabilized by these schemes still fluctuates very much as compared with the two-photon laser frequency of the Raman transition stabilized by the phase-lock or injection-lock scheme. The laser frequency fluctuation is thus an unavoidable problem in the Rydberg-EIT system. In this work, we carry out a systematic theoretical and experimental study of the effects of laser frequency fluctuation on the EIT for laser-cooled ^{87}Rb atoms.

This paper is organized in the following way. In Sec. II, we will derive an analytical formula for the decoherence rate as a function of the laser frequency fluctuation. Since the Doppler shift due to the atomic motion is not negligible in our Rydberg-EIT system, we further include the effect of the Doppler shift in the formula. In Sec. III, we will show how to experimentally test the validity of the formula in the Λ -EIT system. The methods of determination of the coupling Rabi frequency, optical depth, and decoherence rate in the Λ -EIT system will be illustrated in Fig. 3. The laser frequency fluctuation can be controllably introduced to the system. Figure 4 will demonstrate validity of the formula for the frequency fluctuation-induced decoherence rate. In Sec. IV, we will report our study on decoherence processes in the Rydberg-EIT system. The Rydberg state $|32D_{5/2}\rangle$ is selected in the study, because of its negligible DDI effect [47]. Figure 6

will show the result of light-storage measurement, which provides the information on the atom temperature and, consequently, on the Doppler shift-induced decoherence rate. The purpose of Fig. 7 is the same as that of Fig. 3. Figure 8 will compare the measured decoherence rates with the theoretical predictions, and will demonstrate that the theoretical model of this work can describe very well the decoherence processes in the Rydberg-EIT system. Finally, we will make the conclusion in Sec. V.

II. THEORETICAL MODEL

Considering the two transition diagrams in Fig. 1, we derive an analytic formula that relates the decoherence rate of ρ_{21} to the laser frequency fluctuation. In Fig. 1(a), ρ_{21} is the Raman coherence between the two ground states representing the dominant part of the Raman polariton [37, 38]. In Fig. 1(b), ρ_{21} is the coherence between the ground and Rydberg states representing the dominant part of the Rydberg polariton. The logic behind the derivation is the following. Although the laser frequencies are locked to the resonance frequency of the two-photon transition, their fluctuations randomly induce a two-photon detuning to the EIT system. The two-photon detuning results in attenuation or loss of the probe field. An average of the attenuation is equivalent to an increment of the decoherence rate in the system. A larger amplitude of the laser frequency fluctuation represents a greater root-mean-square value of the two-photon detuning, which makes more attenuation, similar to a larger decoherence rate. Therefore, the decoherence rate can be expressed as a function of the fluctuation amplitude.

We employed the optical Bloch equation (OBE) for the density-matrix operator of the atomic ensemble and the Maxwell-Schrödinger equation (MSE) for the probe field in the derivation, giving [48]

$$\frac{\partial}{\partial t}\rho_{21} = \frac{i}{2}\Omega_c\rho_{31} + i\delta\rho_{21} - \gamma_0\rho_{21}, \quad (1)$$

$$\frac{\partial}{\partial t}\rho_{31} = \frac{i}{2}\Omega_p + \frac{i}{2}\Omega_c\rho_{21} + i\Delta_p\rho_{31} - \frac{\Gamma}{2}\rho_{31}, \quad (2)$$

$$\frac{1}{c}\frac{\partial}{\partial t}\Omega_p + \frac{\partial}{\partial z}\Omega_p = i\frac{\alpha\Gamma}{2L}\rho_{31}, \quad (3)$$

where ρ_{21} and ρ_{31} are the density-matrix elements, Ω_p and Ω_c denote probe and coupling Rabi frequencies, γ_0 is the decoherence rate, Γ represents the spontaneous decay rate of the excited state $|3\rangle$ which is $2\pi \times 6.1$ MHz in our case, δ is the two-photon detuning of the Raman or Rydberg transition $|1\rangle \rightarrow |2\rangle$, Δ_p denotes the one-photon detuning of the probe transition $|1\rangle \rightarrow |3\rangle$, and α and L represent the optical depth (OD) and length of the medium.

To achieve the above OBE and MSE, we consider the weak probe field as a perturbation [48], and neglect the effect of dipole-dipole interaction among the Rydberg atoms. Only the slowly-varying amplitudes of the density-matrix elements and those of the probe and coupling Rabi frequencies remain in the equations. All parts

of the equations, except δ , are the same for both the Λ -EIT system shown in Fig. 1(a) and the Rydberg-EIT system shown in Fig. 1(b). The two-photon detuning is $\delta = \Delta_p - \Delta_c$ for the situation shown in Fig. 1(a) and $\delta = \Delta_p + \Delta_c$ for that in Fig. 1(b), where Δ_c is the one-photon detuning of the coupling transition.

To find the EIT spectral profile, we use Eqs. (1) and (2) and obtain the following steady-state solution for ρ_{31} :

$$\rho_{31} = \frac{\delta + i\gamma_0}{\Omega_c^2/2 - 2(\Delta_p + i\Gamma/2)(\delta + i\gamma_0)}\Omega_p. \quad (4)$$

The imaginary and real parts of ρ_{31} determine the output transmission and phase shift of the probe field, respectively. We are only interested in the transmission. Under the typical EIT condition of $\Omega_c^2 \gg 2\gamma_0\Gamma$ and $\Omega_c^2 \gg 4\delta\Delta_p$, the absorption cross section, σ , relates to the imaginary part of ρ_{31} as the following:

$$\sigma(\delta) = \text{Im} \left[\frac{\rho_{31}\Gamma}{\Omega_p} \right] \approx \frac{2\gamma_0\Gamma}{\Omega_c^2} + \frac{4\Gamma^2\delta^2}{\Omega_c^4}. \quad (5)$$

To obtain the steady-state output transmission of the probe field, we drop the time derivative term in Eq. (3), and use the expression of $-[(2\gamma_0/\Omega_c^2) + (4\Gamma\delta^2/\Omega_c^4)]\Omega_p$ for $i\rho_{31}$ on the right-hand side of Eq. (3). After Eq. (3) is solved analytically, one arrives at the following output-to-input ratio or transmission of the probe field as a function of the two-photon detuning:

$$t(\delta) = \frac{|\Omega_p(L)|^2}{|\Omega_p(0)|^2} = e^{-\alpha\sigma(\delta)}. \quad (6)$$

The frequencies of the coupling and probe fields are locked to the resonance frequency of the two-photon transition. However, the frequency fluctuation randomly introduces a two-photon detuning, δ_f to the EIT system. We assume that the random fluctuation has a Gaussian distribution with the e^{-1} half width of Γ_f . The average of transmission due to the Gaussian distribution is

$$\bar{t}(\delta) = \int_{-\infty}^{\infty} d\delta_f \frac{e^{-(\delta_f/\Gamma_f)^2}}{\sqrt{\pi}\Gamma_f} t(\delta + \delta_f). \quad (7)$$

Since reduction of the transmission is equivalent to an increment of the decoherence rate, one can define an effective decoherence rate γ such that $\bar{t}(0) \equiv \exp(-2\alpha\gamma\Gamma/\Omega_c^2)$. After evaluating Eq. (7) at the EIT peak to get $\bar{t}(0)$, we arrive at

$$\gamma = \gamma_0 + \gamma_f,$$

where

$$\gamma_f \equiv \frac{\Omega_c^2}{4\alpha\Gamma} \ln \left(1 + \frac{4\alpha\Gamma^2}{\Omega_c^4} \Gamma_f^2 \right). \quad (8)$$

In this way, the frequency fluctuations add an additional term γ_f to the decoherence rate γ .

Although the sum of the laser frequencies is resonant to the two-photon transition frequency in the lab, a nonzero

two-photon detuning can exist in the frame of moving atoms due to Doppler shift. A higher velocity results in a larger two-photon detuning, δ_D . Since the distribution of the atom velocity is a Gaussian function, the average of the absorption cross section due to the atomic motion is given by [49]

$$\begin{aligned} \bar{\sigma}(\delta) &= \int_{-\infty}^{\infty} d\delta_D \frac{e^{-(\delta_D/\Gamma_D)^2}}{\sqrt{\pi}\Gamma_D} \sigma(\delta + \delta_D) \\ &= \frac{2\gamma_0\Gamma}{\Omega_c^2} + \frac{2\Gamma^2}{\Omega_c^4} \Gamma_D^2 + \frac{4\Gamma^2\delta^2}{\Omega_c^4}, \end{aligned} \quad (9)$$

where Γ_D is the e^{-1} half width of the Gaussian distribution of δ_D . For atoms characterized a temperature T and a mass m , we have

$$\Gamma_D = \Delta k \sqrt{\frac{2k_B T}{m}}. \quad (10)$$

Here k_B is the Boltzmann constant, and $\Delta k = |(\vec{k}_p - \vec{k}_c) \cdot \hat{z}|$ in the Λ -EIT system or $\Delta k = |(\vec{k}_p + \vec{k}_c) \cdot \hat{z}|$ in the Rydberg-EIT system, with \vec{k}_p and \vec{k}_c being the wave vectors of the probe and coupling fields. Note that Γ_D can be negligible in the Λ -EIT system, because the two fields have very similar wavelengths and thus $\Delta k \approx 0$ in the co-propagation configuration of the probe and coupling fields. On the other hand, Γ_D can be significant in the Rydberg-EIT system, because the two fields have rather different wavelengths.

Considering the combined effect of the laser frequency fluctuation and the atomic motion, we substitute $\bar{\sigma}(\delta)$ for $\sigma(\delta)$ in Eq. (6). The evaluation of Eq. (7) at the EIT peak gives the average of transmission, $\bar{t}(0)$. Since the effective decoherence rate, γ , accounts for the reduction of the transmission, i.e., $\bar{t}(0) \equiv \exp(-2\alpha\gamma\Gamma/\Omega_c^2)$, it can be shown that

$$\gamma = \gamma_0 + \gamma_f + \gamma_D, \quad (11)$$

where

$$\gamma_D \equiv \frac{\Gamma}{\Omega_c^2} \Gamma_D^2. \quad (12)$$

Therefore, the total effective decoherence rate γ consists of three parts: the intrinsic decoherence rate of the system γ_0 , the frequency fluctuation-induced decoherence rate γ_f , and the Doppler shift-induced decoherence rate γ_D . Please note again that Γ_f in Eq. (8) is the e^{-1} half width of the Gaussian distribution of frequency fluctuation, and Γ_D in Eq. (12) is that of Doppler shift.

III. EXPERIMENT OF Λ -TYPE EIT

We utilized the Λ -EIT system to verify the formula of the frequency fluctuation-induced decoherence rate γ_f as shown in Eq. (8). The experiment was performed

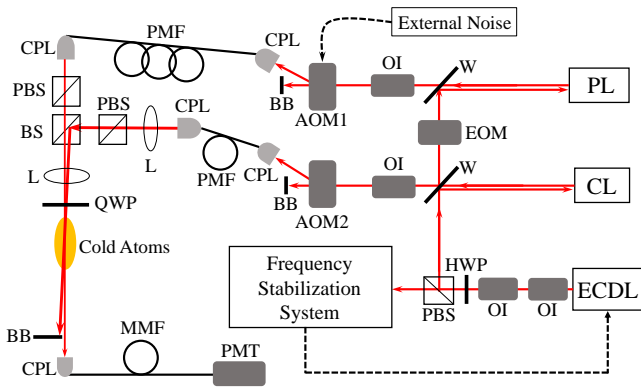


FIG. 2: Experimental setup of the A-EIT study. ECDL: external-cavity diode laser, PL: probe laser, CL: coupling laser, EOM: electro-optic modulator, OI: optical isolator, HWP: half-wave plate, AOM: acousto-optic modulator, BB: beam block, CPL: optical fiber coupler, PMF: polarization-maintained optical fiber, PBS: polarizing beam splitter, BS: beam splitter ($T/R = 10/90$), W: window, L: lens, QWP: quarter-wave plate, MMF: multi-mode optical fiber, and PMT: photo-multiplier tube. Since ECDL injection-locked both of CL and PL, the difference of probe and coupling frequencies was fixed with a high-degree stability. Fluctuation of the two-photon detuning was introduced to the system by AOM1.

with the cigar-shaped cloud of cold ^{87}Rb atoms produced by a magneto-optical trap (MOT) [50]. We optically pumped all population to a single Zeeman state of $|5S_{1/2}, F = 1, m_F = 1\rangle$ before any measurement [51]. In the experiment, both of the probe and coupling fields were σ_+ -polarized. As shown in Fig. 1(a), the probe field drove the transition from $|5S_{1/2}, F = 1, m_F = 1\rangle$ to $|5P_{3/2}, F = 2, m_F = 2\rangle$, and the coupling field drove that from $|5S_{1/2}, F = 2, m_F = 1\rangle$ to $|5P_{3/2}, F = 2, m_F = 2\rangle$. All of the other Zeeman states in the levels of $|5S_{1/2}\rangle$ and $|5P_{3/2}\rangle$ were irrelevant, which can avoid the complexity of multiple EIT subsystems [52, 53]. The wavelengths of probe and coupling fields were all around 780 nm, and their propagation directions were separated by a small angle of about 0.3° . Thus, $\Gamma_D/(2\pi) \approx 1.8$ kHz and the Doppler shift-induced decoherence rate γ_D is negligible.

The experimental setup is shown in Fig. 2. A home-made external-cavity diode laser (ECDL) served as the master laser. We stabilized the ECDL's frequency by the scheme of saturated-absorption spectroscopy. The time constant of feedback loop in the frequency stabilization system was about 3 ms. Since the coupling and probe lasers were seeded or injection-locked by the light beams from the ECDL, their frequency difference was fixed with a high-degree stability. An electro-optic modulator generated 6.8 GHz sidebands in the ECDL beam, and the upper sideband locked the probe laser frequency. Acousto-optic modulators (AOMs) were used to switch the coupling field, generate Gaussian pulses of the probe field, and shift the frequencies of the two fields. As the probe and coupling fields interacted with the atoms, their

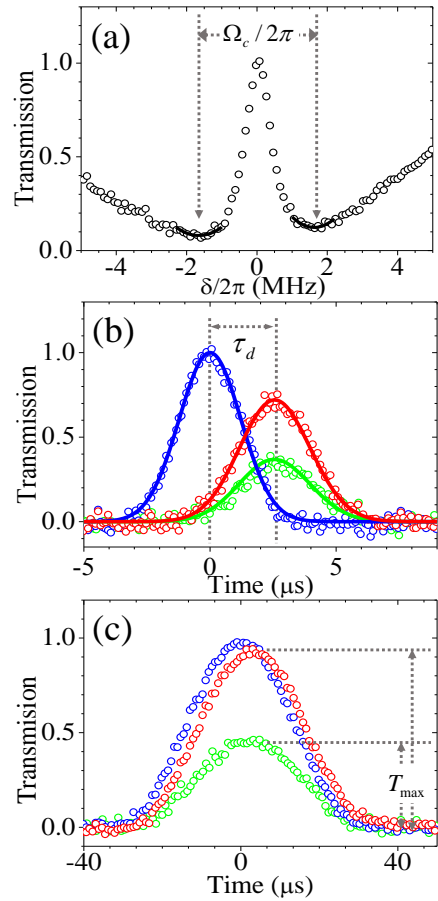


FIG. 3: Determination of experimental parameters in the A-EIT study. In (a), the separation of two transmission minima determines the coupling Rabi frequency. In (b), the delay time determines the optical depth. In (c), the peak transmission of output pulse determines the decoherence rate. Black circles in (a) are the experimental spectrum. Blue circles in (b) and (c) are the experimental data of the input pulse. Red and green circles in (b) and (c) are the output probe pulses without and with frequency fluctuation, respectively. $\Gamma_f/(2\pi)$ of the fluctuation is 280 kHz. Blue line in (b) is the Gaussian best fit, which determined the input pulse width of theoretical calculation. Red (or green) line in (b) is the theoretical prediction calculated with $\Omega_c = 0.54\Gamma$, $\alpha = 29$, and $\gamma = 2.9 \times 10^{-4}\Gamma$ (or $\gamma = 3.9 \times 10^{-3}\Gamma$), determined by the measurements in (a), (b), and (c).

e^{-2} diameters were 0.30 and 4.4 mm, respectively. We set the maximum Rabi frequency of the probe field to about 0.036Γ , which is enough weak to be treated as the perturbation in the theoretical model. A photo-multiplier tube detected the probe light, and its output voltage was recorded by an oscilloscope (Agilent MSO6014A). All the experimental data presented in the paper were averaged for 512 times by the oscilloscope.

The experimental parameters of coupling Rabi frequency (Ω_c), optical depth or OD (α), and effective decoherence rate (γ) were determined in the way illustrated by the example in Fig. 3. First, we measured the separa-

tion of two transmission minima, i.e. the Autler-Townes splitting, to determine Ω_c in Fig. 3(a). The OD was intentionally reduced in the measurement such that the splitting can be clearly observed. We swept the probe frequency by varying the rf frequency of AOM1 shown in Fig. 2. The sweeping rate was 240 kHz/ μ s, which is slow enough not to cause the transient effect [54]. Asymmetry of the spectrum was caused by the decay of OD during the frequency sweeping from low to high two-photon detunings (δ). The value of Ω_c determined in the low-to-high frequency sweeping differed from that in the high-to-low frequency sweeping merely by about 4%. Then, we measured the delay time (τ_d) to determine α in Fig. 3(b), according to $\tau_d = \alpha\Gamma/\Omega_c^2$. A short input pulse with the e^{-1} full width of 3.5 μ s was employed such that the delay time can be determined accurately. Finally, we measured the peak transmission of output pulse (T_{\max}) to determine γ in Fig. 3(c), according to $T_{\max} = \exp(-2\alpha\gamma\Gamma/\Omega_c^2)$. A long input pulse with the e^{-1} full width of 35 μ s at the two-photon resonance was employed to make the result nearly equal to the peak transmission of steady-state EIT window. The red and green lines in Fig. 3(b) are the theoretical predictions. We calculated the predictions by numerically solving Eqs. (1)-(3) with the values of Ω_c , α , and γ determined in the above. The consistency between the experimental data and theoretical prediction demonstrates that the values of Ω_c , α , and γ are convincing.

To verify Eq. (8), we controllably introduced the frequency fluctuation to the system by adding noise to the control signal that set the driving frequency of AOM1. The center frequency of AOM1 kept the probe and coupling frequencies to the resonance of the two-photon transition. Amplitude of the frequency fluctuation was determined by the beat note between the first-order and zeroth-order beams of AOM1. A photo detector (New Focus 1801) detected the beat note and its output signal was sent to a spectrum analyzer (Agilent EXA N9010A). Figure 4(a) shows representative the beat-note spectra measured by the spectrum analyzer. We fitted each spectrum with a Gaussian function. Since the beat note is proportional to the electric field of the first-order beam, Γ_f is equal to the e^{-1} half width of the best fit divided by $\sqrt{2}$.

The frequency fluctuation-induced decoherence rate γ_f is the difference between the decoherence rates γ with and without the frequency fluctuation. Value of γ was determined by the method depicted in Fig. 3(c). In Fig. 4(b), the black squares are the experimental data of γ_f as a function of Γ_f , which is the e^{-1} half width of the Gaussian distribution of frequency fluctuation. In Fig. 4(c), the black, red, and blue squares represent the experimental data of γ_f as functions of the OD at $\Gamma_f/(2\pi)$ of 150, 180, and 220 kHz, respectively. The four lines in Figs. 4(b) and 4(c) represent the theoretical predictions according to Eq. (8), where the calculation parameters of coupling Rabi frequency, OD, and Γ_f were determined by the methods illustrated in Figs 3(a), 3(b), and 4(a). The

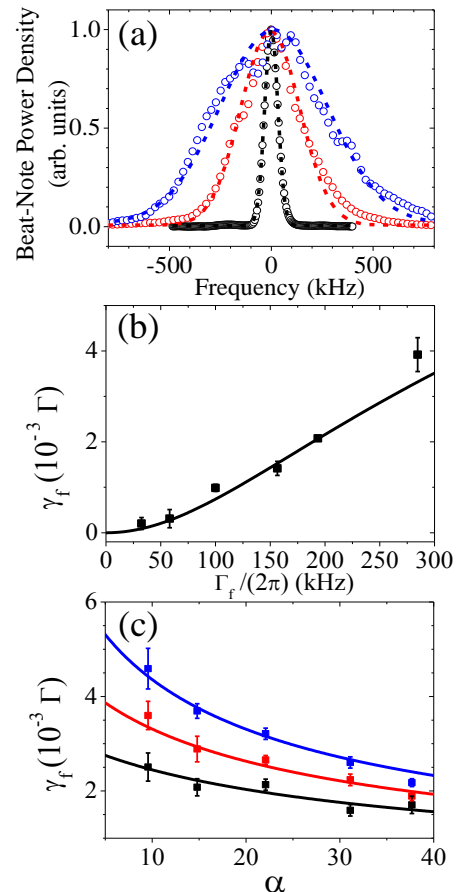


FIG. 4: (a) Representative spectra of the beat note between the first-order and zeroth-order beams of AOM1 in Fig. 2 under different noise amplitudes. Circles are the experimental data and lines are the Gaussian best fits. Since the beat note is proportional to the electric field of the first-order beam, Γ_f is equal to the e^{-1} half width of the best fit divided by $\sqrt{2}$. (b) The decoherence rate γ_f due to the frequency fluctuation as a function of Γ_f . Squares are the experimental data and solid line is the theoretical prediction according to Eq. (8) with experimentally determined Ω_c of 0.54Γ and OD of 29. (c) γ_f as a function of OD. Black, red, and blue squares are the experimental data under $\Gamma_f/(2\pi) = 150, 180,$ and 220 kHz, respectively. Solid lines are the theoretical predictions according to Eq. (8) with experimentally determined Ω_c of 0.44Γ . The values of γ_0 in the measurements of (b) and (c) were $(4.6 \pm 1.4) \times 10^{-4}\Gamma$.

good agreement between the experimental data and the theoretical predictions demonstrates Eq. (8) is valid.

IV. EXPERIMENT OF RYDBERG-STATE EIT

We now study whether Eq. (11) can quantitatively describe the decoherence rate in the Rydberg-EIT system. The experimental study was carried out with the cold ^{87}Rb atoms trapped by the same MOT [50]. We optically pumped all population to a single Zeeman state of

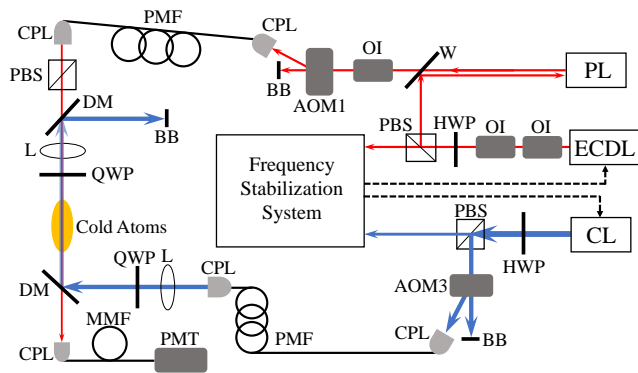


FIG. 5: Experimental setup of the Rydberg-EIT study. ECDL: external-cavity diode laser (Toptica DLC DL pro), PL: probe laser, CL: coupling laser (Toptica TA-SHG pro), OI: optical isolator, W: window, HWP: half-wave plate, PBS: polarizing beam splitter, AOM: acousto-optic modulator, BB: beam block, CPL: optical fiber coupler, PMF: polarization-maintained optical fiber, DM: dichroic mirror, L: lens, QWP: quarter-wave plate, MMF: multi-mode optical fiber, and PMT: photo-multiplier tube. The master laser ECDL seeded PL. In the Frequency Stabilization System, feedback signals from the saturated absorption spectrum and from the Rydberg-EIT spectrum under the Pound-Drever-Hall schemes were used to control the ECDL's and CL's frequencies, respectively. Both spectra were carried out separately in two heated Rb vapor cells.

$|5S_{1/2}, F = 2, m_F = 2\rangle$ before any measurement [55]. In the experiment, both of the probe and coupling fields were σ_+ -polarized. As shown in Fig. 1(b), the probe field drove the transition from $|5S_{1/2}, F = 2, m_F = 2\rangle$ to $|5P_{3/2}, F = 3, m_F = 3\rangle$, and the coupling field drove that from $|5P_{3/2}, F = 3, m_F = 3\rangle$ to $|32D_{5/2}, m_J = 5/2\rangle$. All of the other Zeeman states in the levels of $|5S_{1/2}\rangle$, $|5P_{3/2}\rangle$, and $|32D_{5/2}\rangle$ were irrelevant, which can avoid the complexity of multiple EIT subsystems [52, 53]. We selected a low principle quantum number of $n = 32$ for the Rydberg state such that the DDI effect among Rydberg-state atoms is negligible [47]. The wavelengths of probe and coupling fields were around 780 nm and 482 nm, respectively. They propagated in the opposite directions to minimize the Doppler effect [56]. As the probe and coupling fields interacted with the atoms, their e^{-2} diameters were 300 and 350 μm , respectively. We set the maximum Rabi frequency of the probe field to about 0.034Γ , which is enough weak to be treated as the perturbation in the theoretical model.

The setup of Rydberg-EIT experiment is depicted in Fig. 5. An ECDL (Toptica DLC DL pro) injection-locked or seeded the probe laser. We stabilized the ECDL's frequency by using the Pound-Drever-Hall (PDH) scheme in the saturated-absorption spectrum. The bandwidth of feedback loop for the probe laser in the frequency stabilization system was about 4 MHz. The coupling field was generated by the laser system of Toptica TA-SHG pro. We stabilized the frequency of the coupling laser by

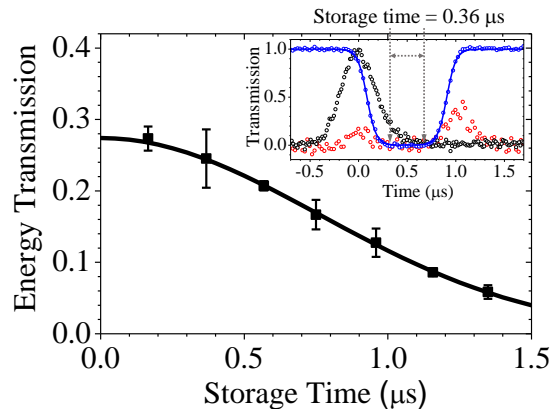


FIG. 6: The main plot shows retrieval efficiency (ratio of output to input energies) of the probe pulse as a function of storage time in the Rydberg-EIT system. Squares are the experimental data of retrieval efficiency measured with $\Omega_c = 1.6\Gamma$ and $\alpha = 30$, and black line is the Gaussian best fit. The coherence time or e^{-1} decay time of the best fit is 1.1 μs , corresponding to the atom temperature of about 350 μK in the experiment. The inset shows representative data. Black and red circles represent the signals of input and output probe pulses. Blue circles represent the signal of coupling field, and blue line is the best fit of the sum of two hyperbolic-tangent functions describing the falling and rising behaviors. We define the storage time as the interval during which the coupling field is completely switched off.

using the PDH scheme in the EIT spectrum, in which light beams from the ECDL and the coupling laser interacted with the atomic vapor in a hot vapor cell [46]. The bandwidth of feedback loop for the coupling laser in the frequency stabilization system was about 50 kHz. We used AOM1 in Fig. 5 to make the probe frequency seen by the cold atoms resonant to or detuned from the transition frequency. Since the coupling frequency seen by the cold atoms was kept resonant to the transition frequency, AOM1 also set the two-photon detuning in the measurement. When the probe and coupling frequencies were both locked, we observed the demodulated PDH signals with a 1 MHz low-pass filter to determine frequency fluctuations of the two stabilization systems. The root-mean-square value of two-photon frequency fluctuation is 150 kHz, indicating $\Gamma_f/(2\pi) = 210$ kHz.

We measured the atom temperature with the Rydberg-EIT light storage to determine Γ_D , which is the e^{-1} half width of the Gaussian distribution of Doppler shift. Figure 6 shows retrieval efficiency (ratio of output to input energies) of the probe pulse as a function of the storage time. The squares are the experimental data and the solid line is the best fit of a Gaussian function. The coherence time or e^{-1} decay time, τ_{coh} of the best fit is 1.1 μs . Since $\tau_{\text{coh}}^{-1} = |\vec{k}_p + \vec{k}_c| \sqrt{k_B T/m}$ [57, 58] and $|\vec{k}_p + \vec{k}_c| = 5.0 \times 10^6 \text{ m}^{-1}$ in our case, the atom temperature was about 350 μK in the Rydberg-EIT experiment. In another measurement of the Λ -EIT light storage, τ_{coh} was 125 μs or the atom temperature was around 350

μK . The two values of atom temperature determined by the Rydberg-EIT and Λ -EIT light storages are consistent. According to the atom temperature of $350 \mu\text{K}$ and Eq. (10), we can know $\Gamma_D/(2\pi) = 200 \text{ kHz}$.

The experimental parameters of coupling Rabi frequency (Ω_c), optical depth or OD (α), and effective decoherence rate (γ) in the Rydberg-EIT system were determined in the similar way as those in the Λ -EIT system. First, we measured the separation of two transmission minima to determine Ω_c in Fig. 7(a). In the measurement, the OD was intentionally reduced and the sweep of probe frequency was done by AOM1 at a speed of $240 \text{ kHz}/\mu\text{s}$ [54]. Then, we measured the delay time (τ_d) to determine α in Fig. 7(b), according to $\tau_d = \alpha\Gamma/\Omega_c^2$. A short input pulse with the e^{-1} full width of $0.53 \mu\text{s}$ was employed. Finally, we measured the transmission as a function of the two-photon detuning to determine the effective decoherence rate γ in Fig. 7(c). A long input pulse with the e^{-1} full width of $7.0 \mu\text{s}$ was employed in each data point. We used a frequency counter (Agilent 53131A), monitoring the rf frequency of the AOM1 in Fig. 5, to determine the two-photon detuning δ .

To determine γ , we fitted the data points in Fig. 7(c) with the fitting function given by

$$\exp \left[-\frac{2\alpha\gamma\Gamma}{\Omega_c^2} - \frac{4\alpha\Gamma^2\delta^2}{\Omega_c^4} - \frac{16\alpha\Gamma^2(2\Omega_c^2 - \Gamma^2)\delta^4}{\Omega_c^8} \right]. \quad (13)$$

Since the absorption cross section in Eq. (5) is valid only around the peak of the EIT spectrum, we need to add the term of δ^4 in the fitting function. The above function is derived by expanding ρ_{31} of Eq. (4) up to δ^4 to obtain the absorption cross section $\sigma(\delta)$, and performing the integrals of Eq. (9) and then Eq. (7). The terms of $(\Gamma_f/\Omega_c)^n$ and $(\Gamma_D/\Omega_c)^n$ with $n \geq 4$ are dropped during the derivation. To fit the data points in Fig. 7(c), Ω_c and α are fixed to the values determined in Figs. 7(a) and 7(b). The solid line in Fig. 7(c) is the best fit that determines the value of γ . The red line in Fig. 7(b) is the theoretical prediction. We calculated the predictions by numerically solving Eqs. (1)-(3) with the values of Ω_c , α , and γ determined in the above. The consistency between the data and prediction in Fig. 7(b) makes the values of coupling Rabi frequency Ω_c , optical depth α , and decoherence rate γ more convincing.

We next studied whether Eq. (11) can quantitatively describe the decoherence processes in our Rydberg-EIT system. The decoherence rates γ at various coupling Rabi frequencies Ω_c were measured. Figure 8 shows γ as a function of $1/\Omega_c^2$. The squares are the experimental data determined by the method illustrated in Fig. 7(c). The dashed lines in Fig. 8 are the theoretical predictions calculated from Eq. (11). In the calculation, we used the values of Ω_c and optical depth (α) determined in Figs. 7(a) and 7(b), and set $\Gamma_f/(2\pi) = 210 \text{ kHz}$, $\Gamma_D/(2\pi) = 200 \text{ kHz}$, and $\gamma_0/(2\pi) = 22 \text{ kHz}$. The value of Γ_f was determined by the demodulated PDH signals in the probe and coupling frequency stabilization systems. The value of Γ_D was determined by the light stor-

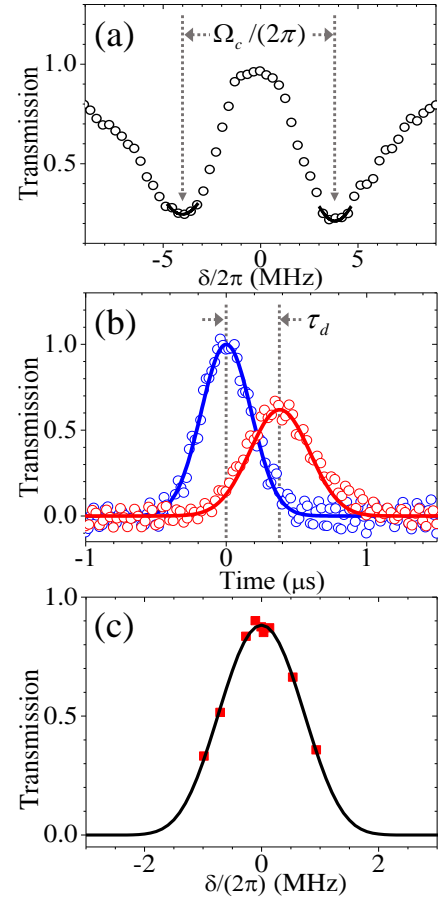


FIG. 7: Determination of experimental parameters in the Rydberg-EIT study. In (a), the separation of two transmission minima determines the coupling Rabi frequency. In (b), the delay time determines the optical depth. In (c), the best fit of data points of transmission versus two-photon detuning determines the decoherence rate. Black circles in (a) are the experimental spectrum. Blue and red circles in (b) are the experimental data of input and output probe pulses. Red squares in (c) are the data of output pulse transmission. Black line in (c) is the best fit with the fitting function shown by Eq. (13). Blue line in (b) is the Gaussian best fit, which determined the input pulse width of theoretical calculation. Red line in (b) is the theoretical prediction calculated with $\Omega_c = 1.3 \Gamma$, $\alpha = 25$, and $\gamma = 4.6 \times 10^{-3} \Gamma$, determined by the measurements in (a), (b), and (c).

age measurement. The value of γ_0 minimizes the difference between the data points and the theoretical predictions. Please note that under $\Omega_c^2/(\Gamma\sqrt{\alpha}) \gg 2\Gamma_f$ where $\Omega_c^2/(\Gamma\sqrt{\alpha})$ is the e^{-1} full width of EIT window, Eq. (8) and Eq. (11) become

$$\gamma_f \approx \frac{\Gamma}{\Omega_c^2} \Gamma_f^2, \quad (14)$$

$$\gamma \approx \gamma_0 + \frac{\Gamma}{\Omega_c^2} (\Gamma_D^2 + \Gamma_f^2). \quad (15)$$

Hence, γ is linearly proportional to $1/\Omega_c^2$ and becomes independent of α at large values of Ω_c as shown in Fig. 8.

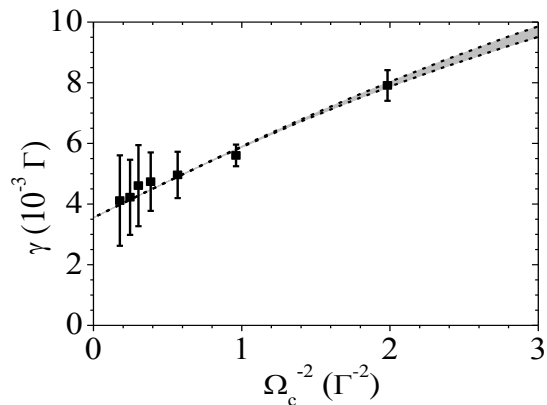


FIG. 8: Decoherence rate of Rydberg polaritons γ as a function of Ω_c^{-2} . Squares are the experimental data determined by the method demonstrated in Fig. 7(c). Top and bottom dashed lines correspond to optical depth (α) = 15 and 26, which were the minimum and maximum values in the measurements. Gray area bound by the two dashed lines, corresponding to various values of α , are the theoretical predictions of Eq. (11) with $\Gamma_D = 2\pi \times 200$ kHz, $\Gamma_f = 2\pi \times 210$ kHz, and $\gamma_0 = 2\pi \times 22$ kHz (or $3.6 \times 10^{-3} \Gamma$).

The good agreement between the data and predictions shows that the theoretical model or Eq. (11) in this work describes the decoherence processes in the Rydberg-EIT system very well.

Finally, one might worry that the separation of two transmission minima, $\Delta\omega_{\text{AT}}$, in Fig. 7(a) and the delay time, τ_d , in Fig. 7(b) can be influenced by the effects of frequency fluctuation and atomic motion. The two effects, i.e., Γ_f and Γ_D , were switched off or negligible in Figs. 3(a) and 3(b), but must be present in Figs. 7(a) and 7(b). Using Eqs. (4), (9), and (7), we derive the values of $\Delta\omega_{\text{AT}}$ and τ_d in the presence of Γ_f and Γ_D . It can be shown that

$$\Delta\omega_{\text{AT}} = \Omega_c \left[1 + \frac{3(\Gamma_f^2 + \Gamma_D^2)}{\Omega_c^2} \right], \quad (16)$$

$$\tau_d = \frac{\alpha\Gamma}{\Omega_c^2} \left[1 + \frac{6(\Gamma_f^2 + \Gamma_D^2)(\Omega_c^2 - \Gamma^2)}{\Omega_c^4} \right]. \quad (17)$$

In our system, $\Gamma_f = 2\pi \times 210$ kHz and $\Gamma_D = 2\pi \times 200$ kHz. The minimum value of Ω_c in this study was 0.71Γ or $2\pi \times 4.3$ MHz. Therefore, $\Delta\omega_{\text{AT}} = \Omega_c$ and $\tau_d = \alpha\Gamma/\Omega_c^2$ used in Figs. 7(a) and 7(b) are the good approximations.

V. CONCLUSION

In this work, we systematically studied the effect of laser frequency fluctuation on the decoherence rate of

the Λ -type and Rydberg-state EIT systems. The laser frequency fluctuation randomly introduces a two-photon detuning to the system, resulting in attenuation of the probe field. The attenuation is equivalent to an increment of the decoherence rate. Using the steady-state solution of the optical Bloch equation and the Maxwell-Schrödinger equation, we derived the formula in Eq. (8) to describe the frequency fluctuation-induced decoherence rate, γ_f . The formula of γ_f was tested in the Λ -EIT system with the laser-cooled ^{87}Rb atoms. The experimental data of γ_f are in the good agreement with the theoretical predictions of Eq. (8).

We further studied the decoherence processes in the Rydberg-EIT system, in which moving atoms induce non-negligible two-photon detunings due to the Doppler shift. We considered the distribution of Doppler shift among the atoms, and obtained the formula in Eq. (12) to describe the Doppler shift-induced decoherence rate, γ_D . The total effective decoherence rate γ shown in Eq. (11) consists of three parts: γ_f , γ_D , and γ_0 , the latter γ_0 being an intrinsic decoherence rate in the system. The experimental study of γ was carried out with the cold atoms of $350 \mu\text{K}$. We utilized the Rydberg state of $|32D_{5/2}\rangle$, in which the dipole-dipole interaction can be neglected. A rather low value of γ of $2\pi \times 48$ kHz was achieved at a moderate coupling Rabi frequency (Ω_c) of $2\pi \times 4.3$ MHz. The experimental data of γ are consistent with the theoretical predictions.

According to Eqs. (8), (11), and (12), larger values of Ω_c make smaller γ . Furthermore, as the EIT linewidth is much greater than the amplitude of the frequency fluctuation, γ is linearly proportional to $1/\Omega_c^2$ and asymptotically approaches to γ_0 . In our Rydberg-EIT system, γ_0 is approximately $2\pi \times 22$ kHz, which comes from the natural linewidth of the Rydberg state, the Lorentzian-type laser linewidths of the probe and coupling fields, and other decoherence processes. The results of our work are useful for the estimation of outcomes or decoherence rates of Rydberg-EIT experiments, and provide a better understanding of the Rydberg-EIT effect.

Acknowledgments

This work was supported by the Ministry of Science and Technology of Taiwan under Grant Nos. 105-2923-M-007-002-MY3, 106-2119-M-007-003, and 107-2745-M-007-001, and the project TAP LIT-2/2016 of the Research Council of Lithuania. JR and GJ also acknowledge a support by the National Center for Theoretical Sciences, Taiwan.

[1] L. Isenhower, E. Urban, X. L. Zhang, A. T. Gill, T. Henage, T. A. Johnson, T. G. Walker, and M. Saffman,

Phys. Rev. Lett. **104**, 010503 (2010).

- [2] T. Wilk, A. Gaëtan, C. Evellin, J. Wolters, Y. Miroshnychenko, P. Grangier, and A. Browaeys, *Phys. Rev. Lett.* **104**, 010502 (2010).
- [3] H. Levine, A. Keesling, A. Omran, H. Bernien, S. Schwartz, A. S. Zibrov, M. Endres, M. Greiner, V. Vuletić, and M. D. Lukin, *Phys. Rev. Lett.* **121**, 123603 (2018)
- [4] M. Saffman and T. G. Walker, *Phys. Rev. A* **66**, 065403 (2002).
- [5] L. Li and A. Kuzmich, *Nat. Commun.* **7**, 13618 (2016).
- [6] H. Weimer, M. Müller, I. Lesanovsky, P. Zoller, and H. P. Büchler, *Nat. Phys.* **6**, 382 (2010).
- [7] H. Kim, Y. J. Park, K. Kim, H.-S. Sim, and J. Ahn, *Phys. Rev. Lett.* **120**, 180502 (2018).
- [8] D. Tong, S. M. Farooqi, J. Stanojevic, S. Krishnan, Y. P. Zhang, R. Côté, E. E. Eyler, and P. L. Gould, *Phys. Rev. Lett.* **93**, 063001 (2004).
- [9] K. Singer, M. Reetz-Lamour, T. Amthor, L. G. Marcassa, and M. Weidemüller, *Phys. Rev. Lett.* **93**, 163001 (2004).
- [10] R. Heidemann, U. Raitzsch, V. Bendkowsky, B. Butscher, R. Löw, L. Santos, and T. Pfau, *Phys. Rev. Lett.* **99**, 163601 (2007).
- [11] A. Gaëtan, Y. Miroshnychenko, T. Wilk, A. Chotia, M. Viteau, D. Comparat, P. Pillet, A. Browaeys, and P. Grangier, *Nat. Phys.* **5**, 115 (2009).
- [12] D. Comparat and P. Pillet, *J. Opt. Soc. Am. B* **27**, A208 (2010).
- [13] A. V. Gorshkov, J. Otterbach, M. Fleischhauer, T. Pohl, and M. D. Lukin, *Phys. Rev. Lett.* **107**, 133602 (2011).
- [14] Y. O. Dudin and A. Kuzmich, *Science* **336**, 887 (2012).
- [15] L. Béguin, A. Vernier, R. Chicireanu, T. Lahaye, A. Browaeys *Phys. Rev. Lett.* **110**, 263201 (2013).
- [16] C. Tresp, C. Zimmer, I. Mirgorodskiy, H. Gorniaczyk, A. Paris-Mandoki, and S. Hofferberth, *Phys. Rev. Lett.* **117**, 223001 (2016).
- [17] F. Ripka, H. Kübler, R. Löw, and T. Pfau, *Science* **362**, 446 (2018).
- [18] M. Fleischhauer, A. Imamoğlu, and J. P. Marangos, *Rev. Mod. Phys.* **77**, 633 (2005).
- [19] C.-K. Chiu, Y.-H. Chen, Y.-C. Chen, I. A. Yu, Y.-C. Chen, Y.-F. Chen, *Phys. Rev. A* **89**, 023839 (2014).
- [20] Z.-Y. Liu, Y.-H. Chen, Y.-C. Chen, H.-Y. Lo, P.-J. Tsai, I. A. Yu, Y.-C. Chen, and Y.-F. Chen, *Phys. Rev. Lett.* **117**, 203601 (2016).
- [21] J. D. Pritchard, D. Maxwell, A. Gauguet, K. J. Weatherill, M. P. A. Jones, and C. S. Adams, *Phys. Rev. Lett.* **105**, 193603 (2010).
- [22] S. Sevinçli, N. Henkel, C. Ates, and T. Pohl, *Phys. Rev. Lett.* **107**, 153001 (2011).
- [23] D. Petrosyan, J. Otterbach, and M. Fleischhauer, *Phys. Rev. Lett.* **107**, 213601 (2011).
- [24] S. Sevinçli, C. Ates, T. Pohl, H. Schempp, C. S. Hofmann, G. Günter, T. Amthor, M. Weidemüller, J. D. Pritchard, D. Maxwell, A. Gauguet, K. J. Weatherill, M. P. A. Jones, and C. S. Adams, *J. Phys. B* **44**, 184018 (2011).
- [25] T. Peyronel, O. Firstenberg, Q.-Y. Liang, S. Hofferberth, A. V. Gorshkov, T. Pohl, M. D. Lukin, and V. Vuletić, *Nature (London)* **488**, 57 (2012).
- [26] B. He, A. V. Sharypov, J. Sheng, C. Simon, and M. Xiao, *Phys. Rev. Lett.* **112**, 133606 (2014).
- [27] O. Firstenberg, C. S. Adams, and S. Hofferberth, *J. Phys. B* **49**, 152003 (2016).
- [28] D. Tiarks, S. Schmidt-Eberle, T. Stolz, G. Rempe and S. Dürr, *Nat. Phys.* **15**, 124 (2018).
- [29] Y.-F. Chen, C.-Y. Wang, S.-H. Wang, and I. A. Yu, *Phys. Rev. Lett.* **96**, 043603 (2006).
- [30] Y.-W. Lin, W.-T. Liao, T. Peters, H.-C. Chou, J.-S. Wang, H.-W. Cho, P.-C. Kuan, and I. A. Yu, *Phys. Rev. Lett.* **102**, 213601 (2009).
- [31] S. Baur, D. Tiarks, G. Rempe, and S. Dürr, *Phys. Rev. Lett.* **112**, 073901 (2014).
- [32] D. Tiarks, S. Schmidt, G. Rempe, and S. Dürr, *Sci. Adv.* **2**, e1600036 (2016).
- [33] K. M. Beck, M. Hosseini, Y. Duan, and V. Vuletić, *Proc. Natl. Acad. Sci. U.S.A.* **113**, 9740 (2016).
- [34] E. Distante, A. Padrón-Brito, M. Cristiani, D. Paredes-Barato, and H. de Riedmatten, *Phys. Rev. Lett.* **117**, 113001 (2016).
- [35] J. Ruseckas, I. A. Yu and G. Juzeliūnas, *Phys. Rev. A* **95**, 023807 (2017).
- [36] C. R. Murray, I. Mirgorodskiy, C. Tresp, C. Braun, A. Paris-Mandoki, A. V. Gorshkov, S. Hofferberth, and T. Pohl, *Phys. Rev. Lett.* **120**, 113601 (2018).
- [37] M. Fleischhauer and M. D. Lukin, *Phys. Rev. Lett.* **84**, 5094 (2000).
- [38] G. Juzeliūnas and H. J. Carmichael, *Phys. Rev. A* **65**, 021601(R) (2002).
- [39] K. J. Weatherill, J. D. Pritchard, R. P. Abel, M. G. Bason, A. K. Mohapatra, and C. S. Adams, *J. Phys. B* **41**, 201002 (2008).
- [40] S. de Léséleuc, D. Barredo, V. Lienhard, A. Browaeys, and T. Lahaye, *Phys. Rev. A* **97**, 053803 (2018).
- [41] R. Legaie, C. J. Picken, and J. D. Pritchard, *J. Opt. Soc. Am. B* **35**, 892 (2018).
- [42] Y. Zeng, K.-P. Wang, Y.-Y. Liu, X.-D. He, M. Liu, P. Xu, J. Wang, and M.-S. Zhan, *J. Opt. Soc. Am. B* **35**, 454 (2018).
- [43] C. J. Picken, R. Legaie, K. McDonnell, and J. D. Pritchard, *Quantum Sci. Technol.* **4** 015011 (2019).
- [44] J. de Hond, N. Cisternas, G. Lochead, and N. J. van Druten, *Appl. Opt.* **56**, 5436 (2017).
- [45] M. Mack, F. Karlewski, H. Hattermann, S. Höckh, F. Jessen, D. Cano, and J. Fortágh, *Phys. Rev. A* **83**, 052515 (2011).
- [46] R. P. Abel, A. K. Mohapatra, M. G. Bason, J. D. Pritchard, K. J. Weatherill, U. Raitzsch, and C. S. Adams, *Appl. Phys. Lett.* **94**, 071107 (2009).
- [47] J. Han, T. Vogt, and W. Li, *Phys. Rev. A* **94**, 043806 (2016).
- [48] S.-C. Gou, S.-W. Su, and I. A. Yu, *Phys. Rev. A* **96**, 047801 (2017).
- [49] S.-W. Su, Y.-H. Chen, S.-C. Gou, T.-L. Horng, and I. A. Yu, *Phys. Rev. A* **83**, 013827 (2011).
- [50] Y.-W. Lin, H.-C. Chou, P. P. Dwivedi, Y.-C. Chen, and I. A. Yu, *Opt. Express* **16**, 3753 (2008).
- [51] Y.-H. Chen, M.-J. Lee, I.-C. Wang, S. Du, Y.-F. Chen, Y.-C. Chen, and I. A. Yu, *Phys. Rev. Lett.* **110**, 083601 (2013).
- [52] Y.-F. Chen, P.-C. Kuan, S.-H. Wang, C.-Y. Wang, and I. A. Yu, *Opt. Lett.* **31**, 3511 (2006).
- [53] T. Peters, Y.-H. Chen, J.-S. Wang, Y.-W. Lin, and I. A. Yu, *Opt. Express* **17**, 6665 (2009).
- [54] Y.-F. Chen, G.-C. Pan, and I. A. Yu, *J. Opt. Soc. Am. B* **21**, 1647 (2004).
- [55] M.-J. Lee, J. Ruseckas, C.-Y. Lee, V. Kudriašov, K.-F. Chang, H.-W. Cho, G. Juzeliūnas, and I. A. Yu, *Nature Commun.* **5**, 5542 (2014).

[56] M. Xiao, Y.-Q. Li, S.-Z. Jin, and J. Gea-Banacloche, Phys. Rev. Lett. **74**, 666 (1995).
[57] B. Zhao, Y.-A. Chen, X.-H. Bao, T. Strassel, C.-S. Chuu, X.-M. Jin, J. Schmiedmayer, Z.-S. Yuan, S. Chen, and J.-

W. Pan, Nat. Phys. **5**, 95 (2009).
[58] S.-W. Su, Y.-H. Chen, S.-C. Gou, and I. A. Yu, J. Phys. B **44**, 165504 (2011).